Chinese Chemical Letters 37 (2026) 112123

Contents lists available at ScienceDirect

Chinese Chemical Letters

journal homepage: www.elsevier.com/locate/cclet

A ROS-scavenging peptide hydrogel combined with mesenchymal stem cells for promoting spinal cord injury recovery

Jun Gu[a,1], Haitao Yuan[a,1], Bo Chu[a], Tianqi Wang[a], Jin Fan[b], Feng Shi[c], Jun Wu[d,*], Xuan Sun[c,*], Xiaojun Feng[a,*]

[a] Department of Orthopedics, Xishan People's Hospital of Wuxi City, Wuxi 214105, China
[b] Department of Orthopedics, the First Affiliated Hospital of NJMU, Nanjing 210029, China
[c] School of Pharmacy, Jiangsu University, Zhenjiang 212016, China
[d] Bioscience and Biomedical Engineering Thrust, The Hong Kong University of Science and Technology (Guangzhou), Guangzhou 511400, China

ARTICLE INFO

Article history:
Received 23 August 2025
Revised 13 November 2025
Accepted 14 November 2025
Available online 15 November 2025

Keywords:
Spinal cord injury
Mesenchymal stem cells
ROS-scavenging hydrogel
BMSC transplantation
Oxidative stress

ABSTRACT

Spinal cord injury (SCI) is a severe neurological disorder often leading to long-term motor dysfunction and permanent disability. Bone marrow-derived mesenchymal stem cell (BMSC) transplantation has been explored to promote SCI recovery; however, the survival and efficacy of transplanted BMSCs are severely compromised by the excessive reactive oxygen species (ROS) present at the injury site. In this study, we developed a peptide hydrogel (MnO_2-Gel) with excellent ROS-scavenging capacity and good biocompatibility. *In vitro* experiments demonstrated that MnO_2-Gel significantly enhanced BMSC survival under oxidative stress conditions. In a rat model of SCI, co-injection of MnO_2-Gel and BMSCs into the lesion site markedly improved locomotor recovery, indicating the potential of this combination strategy for treating SCI.

© 2026 Published by Elsevier B.V. on behalf of Chinese Chemical Society and Institute of Materia Medica, Chinese Academy of Medical Sciences.

Spinal cord injury (SCI) is a systemic disease characterized by central nervous system (CNS) weakness. Globally, there are approximately 27 million individuals living with SCI, with about 9.3 million new cases reported annually [1]. In China, the incidence rate ranges from 25 cases to 60 cases per million people [2]. SCI disrupts neural pathways between the brain and spinal cord, causing severe and often permanent neurological deficits such as sensory and motor impairments, reflex abnormalities, and autonomic dysfunction, ultimately resulting in long-term disability [3]. The challenging clinical management of SCI not only reduces life expectancy but also imposes substantial medical, nursing, and economic burdens on patients and families, leading to significant physical, psychological, and social challenges [4]. Current treatments include early surgical decompression, spinal stabilization, corticosteroid therapy, anti-inflammatory interventions, and rehabilitation training [5], yet their effectiveness remains limited. Therefore, there is an urgent need for novel therapeutic strategies based on a deeper understanding of SCI pathology to improve functional recovery and quality of life for patients.

The pathological process of SCI includes primary injury and secondary injury. After primary injury caused by trauma, a series of secondary damage changes will occur around the injury site, including uncontrolled oxidative stress, severe inflammatory response, leading to necrosis and apoptosis of neurons and glial cells [6,7]. Among these, infiltrating inflammatory immune cells generate excessive reactive oxygen species (ROS), exacerbating neuronal and oligodendrocyte apoptosis [8]. Effective nerve repair after SCI requires not only replenishing lost neurons but also reversing the hostile local microenvironment by providing trophic support and mitigating neurotoxic inflammation and oxidative stress [9].

Cell transplantation has multiple therapeutic capabilities, such as replacing damaged tissue, forming relay neural circuits, immune regulation, neuroprotection, and myelin regeneration, making it a more promising intervention to promote functional improvement after SCI [10]. At present, various types of cells, including mesenchymal stem cells (MSCs), neural stem cells (NSCs), Schwann cells (SCs), have been used to promote the repair of SCI. Among them, bone marrow-derived mesenchymal stem cells (BMSCs) are attractive due to their accessibility, expandability, and lack of ethical concerns. BMSCs exert neuroprotective effects and promote functional recovery in SCI models *via* paracrine signaling and trophic support [11–14]. However, the therapeutic effect of directly transplanted cells is not ideal, as most implanted cells cannot sur-

* Corresponding authors.
E-mail addresses: junwuhkust@ust.hk (J. Wu), xsun61@foxmail.com (X. Sun), featherinwind81@163.com (X. Feng).
[1] These authors contributed equally to this work.

https://doi.org/10.1016/j.cclet.2025.112123
1001-8417/© 2026 Published by Elsevier B.V. on behalf of Chinese Chemical Society and Institute of Materia Medica, Chinese Academy of Medical Sciences.

vive in cytotoxic and inhibitory microenvironments, and excessive ROS production at the site of injury is considered one of the main reasons for this situation [15–18].

Biomaterials capable of scavenging ROS offer a viable approach to modulate the injury microenvironment, protect transplanted cells, and enhance regeneration [8]. Hydrogels, with high water content, biocompatibility, and neural tissue-like properties, can be implanted or injected to fill cavities, support axonal growth, and facilitate cell differentiation without provoking significant immune responses, making them widely applicable in SCI treatment [7,19,20]. For instance, Li *et al.* [8] demonstrated that a ROS-scavenging hydrogel encapsulating BMSCs reduced oxidation, inflammation, and apoptosis, promoted neurogenesis and motor recovery, and diminished scar formation in a rat transection model.

In a variety of gel systems, peptide-based hydrogels have advantages over traditional polymeric hydrogels, such as low immunogenicity, tunable sequences, functional versatility, ease of modification and synthesis, and inherent biocompatibility and biodegradability, making them suitable for drug delivery and regenerative medicine [21,22]. The IKVAV peptide is a core functional motif derived from the laminin $\alpha 1$ chain, a major component of the extracellular matrix [23]. It exhibits significant bioactivity, promoting angiogenesis while inhibiting keratinocyte differentiation and adhesion [24]. Previous studies have shown that hydrogels functionalized with IKVAV can upregulate the expression of angiogenic factors and attenuate the secretion of pro-inflammatory cytokines [25–27]. Moreover, such hydrogels have been reported to suppress glial scar formation at injury sites, thereby fostering a conducive microenvironment for neural regeneration [28]. In this study, we conjugated a diphenylalanine (FF) motif, which is widely employed to provide aromatic π–π stacking interactions for molecular self-assembly [29,30], to the IKVAV peptide to promote peptide self-assembly. Furthermore, C-terminal amidation was introduced to provide additional hydrogen bonding [29], thereby reinforcing the mechanical strength of the crosslinked network. The resulting peptide (FFIKVAV-NH_2), designated as FV peptide, readily self-assembled into a stable hydrogel under physiological conditions. After doping with MnO_2 nanoparticles (NPs), a hydrogel equipped with ROS scavenging capability was successfully fabricated. In a rat model of SCI, the combination of this hydrogel and BMSCs significantly promoted motor recovery and alleviated neurogenic bladder symptoms.

NPs were synthesized through biomineralization using dopamine hydrochloride (DA), potassium permanganate ($KMnO_4$), and bovine serum albumin (BSA) at room temperature [31]: DA undergoes oxidative polymerization to form polydopamine (PDA), while $KMnO_4$ is reduced to MnO_2, leading to co-assembly into MnO_2/PDA NPs (MnO_2 NPs) on the BSA template.

The synthesis conditions were screened (Tables S1–S3 in Supporting information), and MnO_2 NPs was prepared with the optimal formulation to achieve relatively small size and uniform distribution (average diameter: 66.7 ± 0.84 nm; polydispersity index (PDI): 0.153 ± 0.022) (Fig. 1A). The NPs demonstrated good stability in aqueous solution over 7 days (Fig. 1B). Transmission electron microscopy (TEM) revealed a relatively uniform spherical morphology (Fig. 1C). X-ray diffraction (XRD) confirmed the crystal structure of MnO_2, matching the standard pattern (PDF #73–1539) (Fig. 1E). Energy-dispersive X-ray spectroscopy (EDS) mapping showed homogeneous distribution of Mn and O elements (Fig. 1F), verifying the successful preparation of MnO_2 NPs.

Subsequently, FV peptide was synthesized by solid-phase peptide synthesis (SPSS), and its purity was analyzed using high-performance liquid chromatography (HPLC). The chromatographic conditions are shown in Table S4 (Supporting information). HPLC analysis (Fig. S1 in Supporting information) indicated a purity of 96.79 %, exceeding the required threshold of 95 %. LC-MS confirmed

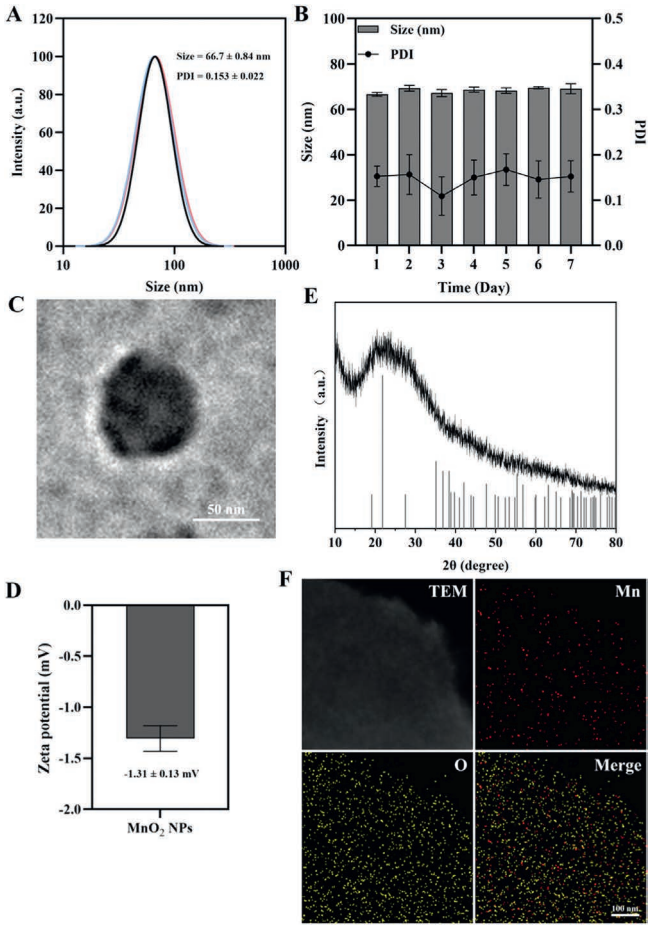


Fig. 1. Preparation and characterization of MnO_2 NPs. (A) Hydrodynamic size distribution and PDI of MnO_2 NPs. (B) Stability assessment of MnO_2 NPs over 7 days. (C) Zeta potential of MnO_2 NPs. (D) Representative TEM image of MnO_2 NPs. Scale bar: 50 nm. (E) XRD pattern of the as-synthesized MnO_2 NPs, with the standard pattern of MnO_2 (PDF #73–1539) shown as a reference. (F) EDS-mapping image of MnO_2 NPs. Scale bar: 100 nm. Data are presented as mean ± standard deviation (SD) ($n = 3$).

the molecular weight ($[M+H]^+$ peak observed at 822.98, which is consistent with the theoretical value 823.05) (Fig. S2 in Supporting information). The above results confirm the successful synthesis of high-purity FV peptide.

The conditions for gelation have been investigated (Tables S5–S7 in Supporting information). The effect of pH on gelation was first investigated (Table S5). No hydrogel formation was observed at pH 5.5; a hydrogel was formed at pH 6.5, but its stability was weak, resulting in a "weak gel, partial flow" characteristic; however, a hydrogel exhibiting good stability with no flow was formed at pH 7.4, indicating that neutral pH conditions favor the self-assembly of the peptide into a stable hydrogel. Next, the effect of peptide concentration on gelation was investigated (Table S6). As expected, the stability of the hydrogel improved with the peptide concentration increased; at concentrations of 25 mg/mL and above, the hydrogel was described as "stable gel, no flow". Finally, the effect of MnO_2 NPs on gelation was studied (Table S7): low concentrations (0.1, 0.2, 0.5 mg/mL) of MnO_2 NPs did not inhibit gelation, while high concentrations (1 and 2 mg/mL) would hinder the self-assembly of peptide.

In summary, we ultimately chose to prepare the hydrogel (Blank-Gel) under the conditions of a peptide concentration of 25 mg/mL and pH 7.4. The hydrogel incorporated with MnO_2 NPs (MnO_2-Gel) was obtained by the same method with 0.5 mg/mL of MnO_2 NPs added. As shown in Fig. 2A, whether MnO_2 NPs are

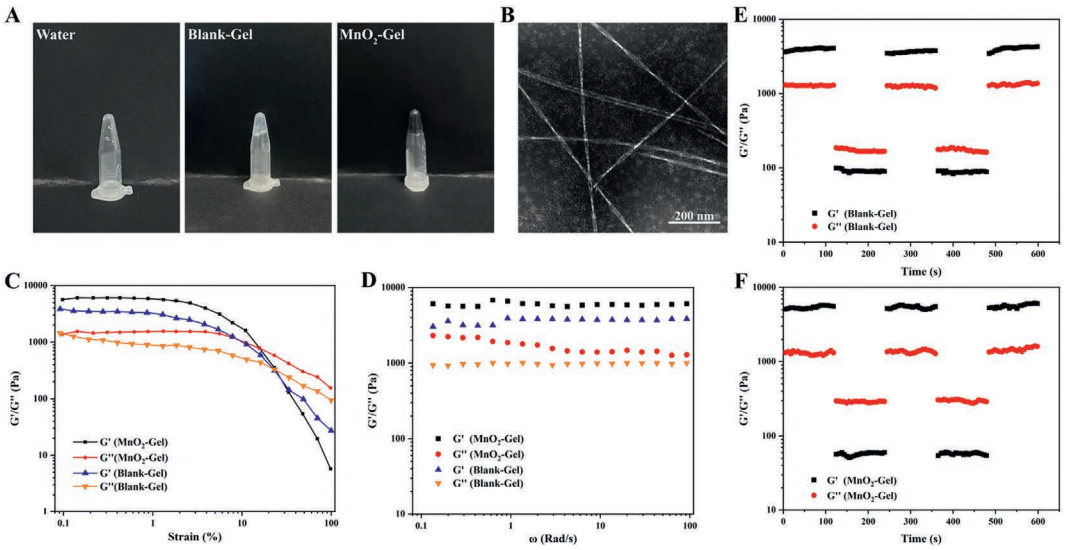


Fig. 2. Characterization of MnO_2-Gel. (A) Photographs of water, Blank-Gel and MnO_2-Gel when inverted. (B) TEM image of Blank-Gel. Scale bar: 200 nm. Rheological test: (C) dynamic strain sweep, (D) dynamic frequency sweep. Cyclic strain time sweep of (E) Blank-Gel and (F) MnO_2-Gel.

added or not, FV peptides formed stable hydrogels that maintained their structure upon inversion. TEM imaging (Fig. 2B) showed that under physiological conditions (pH 7.4), short peptides self-assembled into dense fibrous networks under physiological conditions.

Rheological tests [32] were conducted on Blank-Gel and MnO_2-Gel (Figs. 2C–F). The results of the dynamic strain sweep (Fig. 2C) show that Blank Gel and MnO_2 Gel have similar linear viscoelastic ranges, and both the two exhibited solid-like behavior ($G' > G''$) at low strain, transitioning to fluid-like behavior ($G'' > G'$) at high strain, demonstrating injectability. The G' and G'' value of MnO_2-Gel are slightly higher than those of Blank-Gel, which may be due to due to the electrostatic interactions between negatively charged MnO_2 NPs (-1.31 ± 0.13 mV, Fig. 1D) and positively charged lysine residues (K) in the peptide, which could enhance the strength of the self-assembled structure. Dynamic frequency sweep results (Fig. 2D) show that in the angular velocity range of 100–0.1 rad/s, the G' of Blank-Gel and MnO_2-Gel kept higher than G'', indicating that the mechanical properties of both hydrogels are not affected by frequency. Meanwhile, the G' and G'' value of MnO_2-Gel are slightly higher than those of Blank-Gel, which is consistent with the results of dynamic strain scanning. The results of cyclic strain time sweep (Figs. 2E and F) show that when a low strain force (0.1 %) is applied, the G' of both hydrogels are greater than G'', showing that the hydrogels are solid; When a high strain force (50 %) is applied, the G' and G'' of the two hydrogels are significantly reduced, and G' is less than G'', showing a fluid state which can be injected. Under the alternate action of high and low strain forces, G' and G'' quickly recovered to basically the same level as under the previous round of strain forces, which proved that the hydrogels have good self-healing property.

Next, Blank-Gel and MnO_2-Gel were co-incubated with H_2O_2 (1 mmol/L) and the residual H_2O_2 content in the supernatant was detected using the titanium sulfate [$Ti(SO_4)_2$] colorimetric method [33]. While Blank-Gel showed negligible H_2O_2 degradation (99.35 % remaining), MnO_2-Gel significantly reduced H_2O_2 levels in a concentration-dependent manner, with only 44.41 % remaining at 500 μg/mL MnO_2 NPs (Fig. 3A), confirming that MnO_2-Gel has a certain hydrogen peroxide scavenging ability inherited from MnO_2 NPs.

Before evaluating the ability of MnO_2-Gel to protect BMSCs in oxidative stress microenvironment, its biocompatibility was assessed. As shown in Fig. 3B, when the concentration of MnO_2 NPs varied from 0 (*i.e.*, Blank-Gel) to 500 μg/mL, the cell viability of BMSCs within 24 h was 98.76 %, 98.47 %, 98.03 %, 97.59 %, 96.89 %, 95.63 %, and 91.24 %, respectively. All groups showed cell viability exceeding 90 %, indicating good biocompatibility of MnO_2-Gel.

Next, H_2O_2 (100 μmol/L) was added to the culture medium to simulate the oxidative stress microenvironment of SCI sites. BMSCs were co-incubated with phosphate buffer saline (PBS), Blank-Gel, and MnO_2-Gel, respectively, and the relative cell viability was detected. As shown in Fig. 3C, compared with the Control group (without H_2O_2 added, simulating normal physiological conditions), the relative cell viability in PBS group and Blank-Gel group significantly decreased to 67.01 % and 68.76 % respectively, which were comparable, whereas MnO_2-Gel group maintained significantly higher viability (82.53 %). This indicates that MnO_2-Gel could effectively alleviate the damage of BMSCs in an oxidative microenvironment by scavenging ROS in the microenvironment.

Live/dead (calcein-AM/propidium iodide (PI)) staining was conducted for a more intuitive observation of the survival/death status of BMSCs (Figs. 3D–F). There was almost no cell death in the control group, while cells cultured under oxidative stress microenvironment (PBS, Blank-Gel, MnO_2-Gel groups) showed varying degrees of red fluorescence representing dead cells, with decreased green fluorescence representing live cells. The cell death in MnO_2-Gel group (4.92 %) significantly reduced compared to PBS group (10.94 %) and Blank Gel group (8.95 %), indicating that MnO_2-Gel can alleviate the damage of BMSCs in oxidative stress microenvironment by scavenging ROS.

2′,7′-Dichlorofluorescein diacetate (DCFH-DA) fluorescent probe was used to detect intracellular ROS level in BMSCs under oxidative stress microenvironment. As shown in Figs. 3G and H, cells in the control group only produce a small amount of ROS during normal metabolic processes, so the intensity of green fluorescence representing ROS in the field of view is extremely weak. As expected, DCFH-DA fluorescence of PBS, Blank-Gel and MnO_2-Gel group increased significantly (226.8 %, 220.08 %, and 170.36 % respectively compared to the control group). Moreover, the fluorescence intensity of the MnO_2-Gel group was were significantly lower, indicating that MnO_2-Gel could alleviate the oxidative stress of BMSCs.

As an end-product of lipid peroxidation, malondialdehyde (MDA) serves as a biomarker reflecting the extent of oxidative

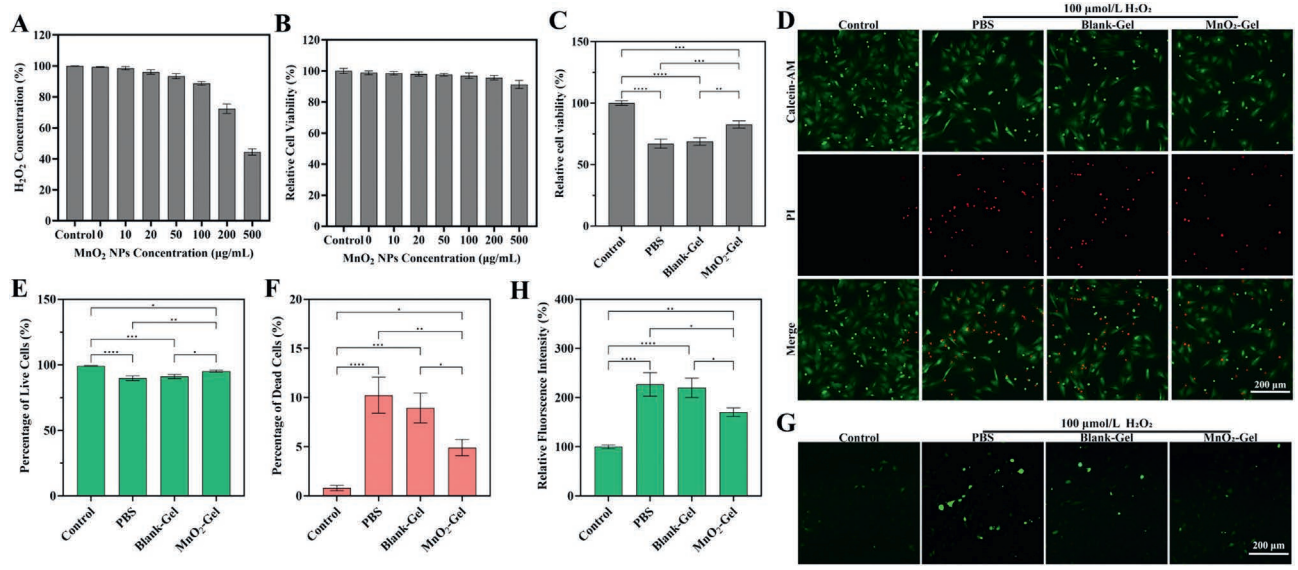


Fig. 3. MnO_2-Gel protects BMSCs against oxidative stress *in vitro*. (A) Quantification of the remaining H_2O_2 content after 2 h of co-incubation with MnO_2-Gel. (B) Relative viability of BMSCs after 24 h co-culture with hydrogels containing the indicated concentrations of MnO_2 NPs. (C) Relative viability of BMSCs after 24 h of different treatment under H_2O_2-induced oxidative stress. (D) Representative fluorescence images of BMSCs stained with calcein-AM (live, green) and PI (dead, red) following respective treatments. Semi quantitative analysis of (E) calcein-AM and (F) PI fluorescence intensity. (G) Representative fluorescence images of intracellular ROS levels detected by the DCFH-DA probe. Scale bar: 200 μm. (H) Semi quantitative analysis of DCFH-DA fluorescence intensity. Data are represented as mean ± SD ($n = 3$). $^{*}P < 0.05$, $^{**}P < 0.01$, $^{***}P < 0.001$, $^{****}P < 0.0001$.

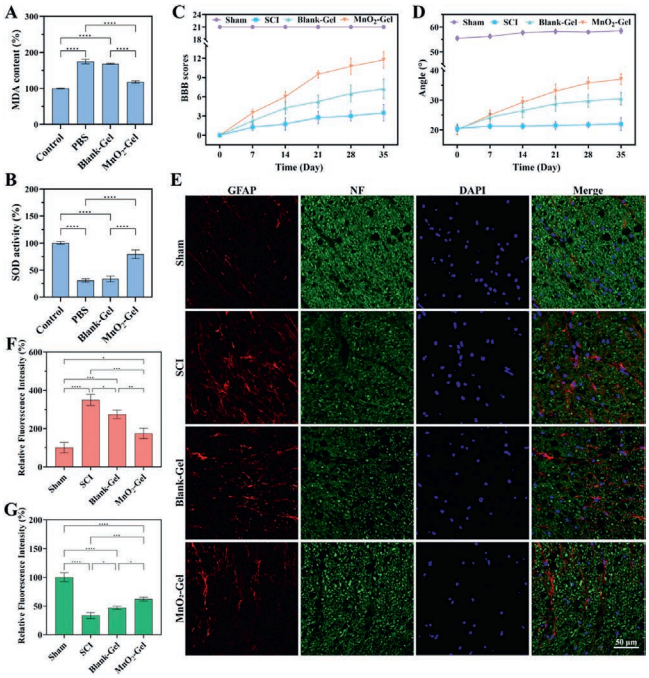


Fig. 4. (A) Intracellular MDA content in BMSCs under oxidative stress. (B) SOD activity in BMSCs under oxidative stress. (C–G) MnO_2-Gel synergizes with BMSCs to promote functional and histological recovery after SCI *in vivo*: (C) Hindlimb motor function recovery of rats evaluated through BBB scores; (D) Hindlimb strength recovery of rats measured by the maximum angle maintained on an inclined plane; (E) representative immunofluorescence images of spinal cord sections stained for GFAP (glial scar marker, red) and neurofilament (NF, axonal marker, green) (scale bar: 50 μm); semi quantitative analysis of (F) GFAP and (G) NF fluorescence intensity. Data are represented as mean ± SD ($n = 4$). $^{*}P < 0.05$, $^{**}P < 0.01$, $^{***}P < 0.001$, $^{****}P < 0.0001$.

damage in cells. As shown in Fig. 4A, the MDA content in BMSCs was elevated to varying degrees in the PBS, Blank-Gel, and MnO_2-Gel groups compared to the control group, indicating oxidative stress-induced cellular injury. Notably, the increase in MDA content was comparable between the PBS and Blank-Gel groups, whereas the MnO_2-Gel group showed a significantly attenuated rise in MDA, demonstrating the protective role of MnO_2-Gel against ROS-mediated oxidative stress. Furthermore, we assessed the activity of superoxide dismutase (SOD), a key antioxidant enzyme that mitigates oxidative damage (Fig. 4B). Consistent with the MDA results, SOD activity decreased across all treatment groups; however, the MnO_2-Gel group maintained significantly higher SOD activity compared to both the PBS and Blank-Gel groups, further supporting the antioxidative efficacy of MnO_2-Gel.

In order to investigate whether MnO_2-Gel could enhance the therapeutic effect of BMSCs transplantation therapy, we constructed a rat gravity-strike SCI model. This work was approved by the Institutional Animal Care and Use Committee of Jiangsu University (No. UJS-IACUC-2025,030,702). Treatments included: MnO_2-Gel + BMSCs (MnO_2-Gel group); Blank-Gel + BMSCs (Blank-Gel group); PBS (SCI group). In addition, a sham surgery group (sham group) without gravity impact served as control.

The Basso-Beattie-Bresnahan (BBB) score is a scoring system used to assess the level of hind limb motor function after SCI in rats (BBB scoring criteria were shown in Table S8 in Supporting information). The score ranges from 0 to 21, with 0 indicating no visible hind limb movement and 21 indicating normal motor function. As shown in Fig. 4C, rats lost motor function after injury (BBB score = 0); over 5 weeks, the SCI group showed minimal recovery (BBB = 3.25 ± 1.29); both cell-transplanted groups exhibited improvement due to the therapeutic effect of BMSCs transplanted to the injury site, with the MnO_2-Gel group (11.25 ± 1.26) achieving significantly better recovery than the Blank-Gel group (7.25 ± 1.5), which could be attributed to the fact that MnO_2-Gel could scavenge the excess ROS at the injury site, thus enhancing the therapeutic effect of transplanted BMSCs and promoting the recovery of SCI.

The inclined plate test is an important supplement to BBB score, which can compensate for the shortcomings of a single evaluation method and effectively improve the accuracy of scoring. The larger the angle, the stronger the hind limb strength of the rat. The inclined plane test (Fig. 4D) yielded consistent results to BBB

score. After gravitational impact on the spinal cord of rats, the hind limbs lost their weight-bearing capacity and the maximum angle at which they could stay on the inclined plate decreased to 18°–22°. Within the next 5 weeks, there was almost no recovery in the weight-bearing capacity of the hind limbs of SCI group rats; the maximum holding angle was significantly higher in the MnO_2-Gel group (37° ± 1.83°) than in the Blank-Gel group (30.5° ± 2.08°) or SCI group (22° ± 2.16°), indicating rats in the MnO_2-Gel group exhibited stronger hind limb strength.

Immunofluorescence staining was used to detect the expression of glial fibrillary acidic protein (GFAP) in astrocytes and neurofilament protein (NF) in mature neurons in spinal cord tissue, in order to comprehensively evaluate the repair of neural tissue. The two showed a negative correlation. As shown in Figs. 4E–G, the GFAP signal in the sham group was very weak while the NF signal was strong. This is because the spinal cord tissue of the Sham group rats was not damaged by gravity strikes; the SCI group showed significant GFAP signals and a significant decrease in NF signals, indicating that the activation of astrocytes at the site of injury resulted in a large number of glial scars, which prevented axonal regeneration; compared with the SCI group, the GFAP signal in the Blank-Gel group and MnO_2-Gel group was weakened, while the NF signal was enhanced. This is due to the fact that transplanted BMSCs filled the injury site and exerted their paracrine effects, preventing glial scar enlargement and promoting axonal regeneration. In addition, the GFAP signal of the MnO_2-Gel group is weaker than that of the Blank-Gel group while the NF signal intensity is stronger, because MnO_2-Gel can clear excess ROS generated at the site of injury, thereby improving the survival of transplanted cells and enabling them to better exert therapeutic effects.

Neurogenic bladder refers to the dysfunction of the bladder and urethra caused by damage to the CNS or peripheral nerves that control urination function. It is one of the most serious complications of SCI and seriously affects the quality of life of patients with SCI. Masson and hematoxylin-eosin (H&E) staining (Figs. S3A and B in Supporting information) revealed weak bladder contraction, significant thickening and even adhesion of the bladder wall in the SCI group due to SCI, which was attenuated in both BMSC-treated groups, with MnO_2-Gel showing superior improvement.

In order to evaluate the biocompatibility of MnO_2-Gel, H&E staining was performed on the main organs of rats (heart, liver, spleen, lungs, kidneys) (Fig. S3C in Supporting information), and no significant neutrophil infiltration or pathological damage was found. Among them, there was no obvious edema of renal tubular epithelial cells in the rat kidney tissue, which was because manual pressing of the rat bladder every day after modeling avoided serious urinary retention, so no further urinary complications were caused. In addition, blood samples were collected for routine biochemical index testing (Figs. S3D–G in Supporting information). The alanine aminotransferase (ALT), aspartate aminotransferase (AST), blood urea nitrogen (BUN), and creatinine (CR) levels of SCI group rats were all higher because in this group rats did not receive effective treatment, and the negative effects of urinary dysfunction on liver and kidney function cannot be completely eliminated by only assisted urination. Meanwhile, there was no significant difference in various indicators among Blank-Gel group, MnO_2-Gel group and Sham group. The above results indicate that both Blank-Gel and MnO_2-Gel have good biocompatibility.

SCI remains a formidable challenge in clinical practice, primarily due to the highly hostile microenvironment at the lesion site that compromises the efficacy of regenerative therapies. While BMSC transplantation holds great promise, its therapeutic potential is severely limited by the excessive ROS. In this study, we integrated manganese dioxide NPs with ROS-scavenging ability into a self-assembling IKVAV-functionalized peptide hydrogel to obtain MnO_2-Gel. This design aims to simultaneously scavenge ROS and leverage the inherent bioactivity of the IKVAV motif to enhance BMSCs therapy. *In vitro* experiments have shown that MnO_2-Gel demonstrate excellent biocompatibility, and could eliminate excess ROS in the microenvironment to alleviate oxidative stress damage of BMSCs. *In vivo*, it could enhance the therapeutic outcomes of BMSCs transplantation by inhibiting glial scar formation, promoting axonal regeneration, improving motor function, and mitigating neurogenic bladder pathology in a rat SCI model. In conclusion, we present a strategically designed peptide hydrogel that protects transplanted BMSCs from oxidative stress and concurrently provides a therapeutically beneficial IKVAV signal. This study highlights the value of multi-targeted biomaterial strategies to augment cell-based therapies for SCI by actively correcting the pathological microenvironment. This represents a promising and safe candidate for future translational research.

CRediT authorship contribution statement

Jun Gu: Writing – original draft, Project administration, Methodology, Investigation. **Haitao Yuan:** Project administration, Methodology, Investigation. **Bo Chu:** Project administration. **Tianqi Wang:** Software, Resources. **Jin Fan:** Software, Resources. **Feng Shi:** Validation, Software. **Jun Wu:** Writing – review & editing, Supervision, Funding acquisition, Conceptualization. **Xuan Sun:** Writing – review & editing, Supervision, Funding acquisition. **Xiaojun Feng:** Writing – review & editing, Supervision, Funding acquisition.

Declaration of competing interest

The authors declare that they have no known competing financial interests or personal relationships that could have appeared to influence the work reported in this paper.

Acknowledgments

This work was supported by 2022 Jiangsu Provincial Health and Wellness Commission Surface Project (No. M2022026), 2022 Wuxi Municipal Health Commission Key Discipline Innovation Teams (No. CXTD2021022) and Wuxi Municipal Health Commission Project (No. Q202215).

Supplementary materials

Supplementary material associated with this article can be found, in the online version, at doi:10.1016/j.cclet.2025.112123.

References

[1] J.H. Badhiwala, J.R. Wilson, M.G. Fehlings, Lancet Neurol. 18 (2019) 24–25.
[2] H. Shen, C. Fan, Z. You, et al., Adv. Funct. Mater. 32 (2021) 2110628.
[3] C. Ehrmann, S.M. Mahmoudi, B. Prodinger, et al., J. Rehabil. Med. 52 (2020) jrm00037.
[4] A. Alizadeh, S.M. Dyck, S. Karimi-Abdolrezaee, Front. Neurol. 10 (2019) 282.
[5] M. Karsy, G. Hawryluk, Curr. Neurol. Neurosci. Rep. 19 (2019) 65.
[6] M.E. Schwab, D. Bartholdi, Physiol. Rev. 76 (1996) 319–370.
[7] W. Chi, R. Liu, W. Zhou, et al., Chin. Chem. Lett. 36 (2025) 110587.
[8] Z. Li, T. Zhao, J. Ding, et al., Bioact. Mater. 19 (2023) 550–568.
[9] D. Liu, G. Lu, B. Shi, et al., Adv. Healthc. Mater. 12 (2023) e2300123.
[10] P. Assinck, G.J. Duncan, B.J. Hilton, et al., Nat. Neurosci. 20 (2017) 637–647.
[11] S. Papa, I. Vismara, A. Mariani, et al., J. Control. Rel. 278 (2018) 49–56.
[12] T. Cao, H. Chen, W. Huang, et al., Theranostics 12 (2022) 3057–3078.
[13] C.P. Hofstetter, E.J. Schwarz, D. Hess, et al., Proc. Natl. Acad. Sci. U. S. A. 99 (2002) 2199–2204.
[14] O. Albayrak, T.E. Sener, M. Ersahin, et al., Int. J. Impot. Res. 32 (2020) 308–316.
[15] W. Xu, L. Chi, R. Xu, et al., Spinal Cord. 43 (2005) 204–213.
[16] V. Neirinckx, D. Cantinieaux, C. Coste, et al., Stem. Cells 32 (2014) 829–843.
[17] L. Li, B. Xiao, J. Mu, et al., ACS Nano 13 (2019) 14283–14293.
[18] Z. Liu, X. Yao, W. Jiang, et al., J. Neuroinflammat. 17 (2020) 90.
[19] A. Marchini, A. Raspa, R. Pugliese, et al., Proc. Natl. Acad. Sci. U. S. A. 116 (2019) 7483–7492.
[20] R.C. Assuncao-Silva, E.D. Gomes, N. Sousa, et al., Stem Cells Int. 2015 (2015) 948040.

[21] S. Eskandari, T. Guerin, I. Toth, et al., Adv. Drug Deliv. Rev. 110-111 (2017) 169–187.
[22] W. Zhang, H. Wu, L. Xie, et al., Chin. Chem. Lett. 36 (2025) 110800.
[23] B. Li, T. Qiu, P. Zhang, et al., Cell Prolif. 47 (2014) 133–145.
[24] A.E. Haggerty, M. Oudega, Neurosci. Bull. 29 (2013) 445–459.
[25] M.B. Orr, J.C. Gensel, Neurotherapeutics 15 (2018) 541–553.
[26] T. Kanemoto, R. Reich, L. Royce, et al., Proc. Natl. Acad. Sci. U. S. A. 87 (1990) 2279–2283.
[27] K. Tashiro, G.C. Sephel, B. Weeks, et al., J. Biol. Chem. 264 (1989) 16174–16182.
[28] Y. Chai, Y. Long, X. Dong, et al., Colloids Surf. B 210 (2022) 112220.
[29] M.J. Webber, E.T. Pashuck, Adv. Drug Deliv. Rev. 172 (2021) 275–295.
[30] M. Reches, E. Gazit, Science 300 (2003) 625–627.
[31] B. Xiao, X. Zhou, H. Xu, et al., ACS Nano 12 (2018) 12682–12691.
[32] Y. Wu, Z. Wang, Y. Ge, et al., J. Control. Rel. 370 (2024) 747–762.
[33] Y. Zhao, S. Song, D. Wang, et al., Nat. Commun. 13 (2022) 6758.